

Molecular modeling of metastable FeB₄₉ phase evolution in laser surface engineered coating

K. Balani and A. Agarwal^{a)}

Department of Mechanical and Materials Engineering, Florida International University, EAS 3400, Miami, Florida 33174

Narendra B. Dahotre

Department of Materials Science and Engineering, The University of Tennessee, Knoxville, Tennessee 37996 and Materials Processing Group, Metals and Ceramic Division, Oak Ridge National Laboratory, Oak Ridge, Tennessee 37831

(Received 3 August 2005; accepted 17 January 2006; published online 17 February 2006)

Interstitial iron-boride phases have been a subject of research interest for a long time owing to their useful properties. Metastable FeB₄₉ phase evolved during nonequilibrium laser surface engineering was investigated along with FeB, Fe₂B, and Fe₃B phases. Theoretical x-ray diffraction spectrum derived from numerically constructed FeB₄₉ crystal matched with the experimental diffraction pattern from laser surface engineered boride coating on the steel substrate. Furthermore, employment of *ab initio* SIESTA 1.3 molecular modeling for computation of total crystal energy elucidated instability of the FeB₄₉ phase. The generation of thermodynamically nonequilibrium phase FeB₄₉ along with Fe₃B phase was further confirmed by selected area diffraction and high-resolution transmission electron microscopy analyses. © 2006 American Institute of Physics. [DOI: 10.1063/1.2172704]

I. INTRODUCTION

Lasers have been used for surface modification for improvement in material properties such as resistance to wear, friction, erosion, fatigue, corrosion, and high-temperature oxidation.^{1–4} Laser material processing involves extremely high cooling rate (10⁵–10⁸ K/s) that results in the generation of metastable and nonequilibrium phases due to extended solid solubility. It is often observed that these phases are unknown to equilibrium phase diagram.^{1–6}

In our earlier work, we have synthesized TiB₂ coating on AISI 1010 steel substrate using a 2.5 kW continuous wave neodymium-doped yttrium aluminum garnet (Nd:YAG) laser.^{1,2,4} Rapid cooling and solidification during laser processing generated “composite” coating consisting of borides in iron-rich matrix. TiB₂ was the major phase along with TiB and iron borides such as FeB, Fe₃B, and FeB₄₉.^{1,2,4}

In continuation of the above mentioned efforts, in the present work, phases of iron-boride system (FeB, Fe₂B, Fe₃B, and FeB₄₉ phases) were considered for *ab initio* total energy simulation using SIESTA 1.3 (Spanish initiative for electronic simulations with thousands of atoms) molecular modeling package. Evolution of rarely reported metastable FeB₄₉ phase was further validated employing high-resolution transmission electron microscopy (HRTEM). An effort was made to compare these phases with theoretically generated Fe–B phases and correlate the total energy to the relative stability of the structure.

Apart from major TiB₂ peaks, experimental x-ray diffraction (XRD) spectrum depicted some extra peaks corresponding to metastable phases.^{1,2,4} These extra peaks were

identified for Fe₃B, FeB₄₉, and Fe_{2.12}B_{103.39} phases. The experimentally obtained XRD pattern was compared with theoretically computed XRD pattern (Fig. 1) for confirmation of the presence of FeB₄₉ and Fe_{2.12}B_{103.38} phases. FeB₄₉ crystal construction [Fig. 2(a)] and its computed XRD pattern were obtained using CARINE 3.1 (Divergents A, Compiegne, France) crystallographic software. The strongest peak corresponding to FeB₄₉ appeared to be overlapped by (001) peak of TiB₂. Even though Table I presented lattice parameters of various phases in laser synthesized composite coating, the primary interest of the present study resides with the characterization of metastable FeB₄₉ phase, which so far is not reported in the open literature.^{7–9}

Thermodynamic calculations have shown that the free energy of TiB₂ is the least and therefore is a most stable

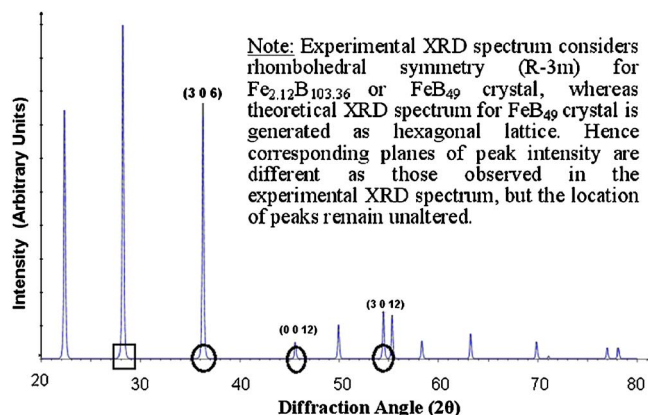


FIG. 1. (Color online) Theoretical x-ray diffraction spectrum of FeB₄₉ crystal as seen in Fig. 2(a). All the experimental peaks for FeB₄₉ phase are matched with circles. The peak marked with rectangle overlapped with major (001) peak of TiB₂.

^{a)}Author to whom correspondence should be addressed; electronic mail: agarwala@fiu.edu

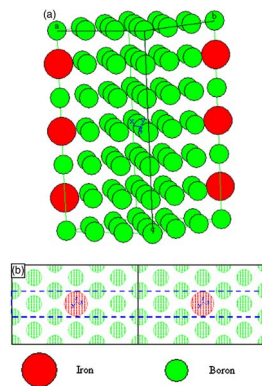


FIG. 2. (Color online) (a) Crystal structure of FeB_{49} and (b) pipe structure along (002) of FeB_{49} crystal.

phase among the Ti–B and Fe–B boride systems.¹⁰ Moreover, free energy curves of the formation of TiB_2 , TiB, FeB, and Fe_2B are almost independent of temperature. The free energies of the formation of TiB_2 , TiB, FeB, and Fe_2B are -319.7 , -159.7 , -31.8 , and -26.0 kJ/mole, respectively.^{8,10} It is evident from the Fe–B phase diagram that FeB and Fe_2B are the equilibrium boride phases.^{8,9,11} Apart from limited studies on Fe_3B (enthalpy of -17.8 kJ/mole) there are no additional thermodynamic data available for the metastable phases of Fe–B system such as Fe_3B , FeB_{49} , and $\text{Fe}_{2.12}\text{B}_{103.38}$. Since the crystal energy is defined by per atom contribution, $\text{Fe}_{2.12}\text{B}_{103.38}$ crystal energy is similar to that of FeB_{49} crystal and, therefore, it was not calculated separately for both crystals. No computational work has been ever carried out for modeling FeB_{49} crystal energy.^{7-9,11} Hence, to extend the knowledge about the relative stability of generated Fe–B phases to the next level of understanding, their total crystal energies were computed and compared.

II. CRYSTAL CONSTRUCTION OF METASTABLE FeB_{49} PHASE AND GENERATION OF THEORETICAL X-RAY DIFFRACTION SPECTRUM

The crystal structure of FeB_{49} was experimentally determined using the JADE 3.1 software (Materials Data, Inc., Livermore, CA, USA), which provided the lattice parameters of $10.95 \times 10.95 \times 23.86 \text{ \AA}^3$, confirming to $R-3m$ crystal symmetry.^{10,12,13} A crystal construction was carried out using CARINE 3.1 [Fig. 2(a)]. The corresponding theoretical XRD spectrum derived earlier (Fig. 1), along with the crystal structure determined by CARINE 3.1, substantiated the experimental peaks for the FeB_{49} crystal. The crystal is defined as

TABLE I. Crystal structure and lattice parameters for various phases (Refs. 2, 6, 7, and 9).

Phase	Structure	Space group	Unit cell (\AA)
TiB_2	Hexagonal	$P6/mmm$	$a=3.03, c=3.23$
FeB	Orthorhombic	$Pnma$	$a=5.51, b=2.95, c=4.06$
Fe_2B	BCT	$I4/mcm$	$a=5.11, c=4.249$
Fe_3B	Tetragonal	$P42/n$	$a=8.69, c=4.31$
FeB_{49}	Rhombohedral	$R-3m$	$a=10.95, c=23.86$
$\text{Fe}_{2.12}\text{B}_{103.38}$	Rhombohedral	$R-3m$	$a=10.95, c=23.861$

rhombohedral structure with lattice constants $a=9.4983 \text{ \AA}$ ($=b \neq c$) and $\alpha=65.22$ ($=\beta \neq \gamma$) using CARINE 3.1 crystallographic software. This crystal structure satisfied the stoichiometry for the crystal of the metastable phase, FeB_{49} (or $\text{Fe}_{2.12}\text{B}_{103.36}$), with lattice constants of $10.95 \times 10.95 \times 23.86 \text{ \AA}^3$, confirming to the rhombohedral space group ($R-3m$) that was experimentally determined from laser engineered coating using JADE software. A hexagonal crystal symmetry ($10.95 \times 10.95 \times 23.86 \text{ \AA}^3$) can be reoriented vice versa as a rhombohedral crystal symmetry with a lattice constant of 9.4983 \AA ($\alpha=65.22$), hence experimental lattice constants for both the crystal structures correspond to the same FeB_{49} phase. Plane (002) of FeB_{49} crystal is represented in Fig. 2(b), indicating that Fe is symmetrically enclosed in a pipe structure of B atoms.⁶

III. IMPLEMENTATION OF SIESTA 1.3 FOR AB INITIO MOLECULAR MODELING OF FE–B SYSTEM

The crystallographic models for FeB, Fe_2B , Fe_3B , and FeB_{49} (referred to as Fe–B system) were chosen from the available theoretical calculations of the unit cell.^{7,9} With $2 \times 2 \times 2$ cell size, a plane wave basis set with periodic boundary conditions was used for Fe–B system because of the periodic nature of the crystalline phases.^{7-9,11} Kohn-Sham self-consistent density functional method along with linear combination of atomic orbital (LCAO) basis set was used in the *ab initio* SIESTA 1.3 package for electronic simulation of Fe–B system.¹⁴ Spin-polarized Ceperley-Alder scheme (by Perdew and Zunger) was adopted both for Fe and B exchange correlation functionals.¹⁴ The interaction between core and valence electrons was described by nonlocal, norm-conserving “improved Troullier-Martins” approach for generating pseudopotentials.¹⁴

As a first principle, iron (Fe) and boron (B) pseudopotentials were generated from spin-polarized and nonrelativistic ground states with components expressed Kleinman and Bylander projectors.¹⁴ Fe was represented by a ground state as $4s^2 4p^0 3d^6 4f^0$ with cutoff core radii of 2.00, 2.00, 2.00, and 2.00 bohrs, respectively, with the core radii of 0.7 bohr.¹⁵ Whereas B was represented by $2s^2 2p^1 3d^0$ with cutoff core radii of 1.78, 1.89, and 1.89 bohrs, respectively.¹⁶ A mesh cutoff energy for the grid was set to 100 Ry, which was optimized automatically by SIESTA 1.3 during its run. Diagonalization method was used in calculations of the localized spin density (LSD) Hamiltonian to generate a self-consistent Kohn-Sham solution. Coordinate optimization by conjugate gradient (CG) was utilized for molecular dynamics run with the limit of total force converging less than 0.05 eV/\AA or 50 iterations (except for FeB_{49} , where maximum iterations used were 20), whichever came first. Maximum displacement during CG optimization run was set at 0.2 bohr.

Molecular modeling results (Fig. 3) indicated the utmost stability of the FeB phase followed by Fe_2B , Fe_3B , and FeB_{49} phases. Since the absolute total energy of the phases is negative, higher-energy ratios dictate the higher stability of the phases. To persist the apt evaluation of generated phases, normalization was carried out with respect to the total energy

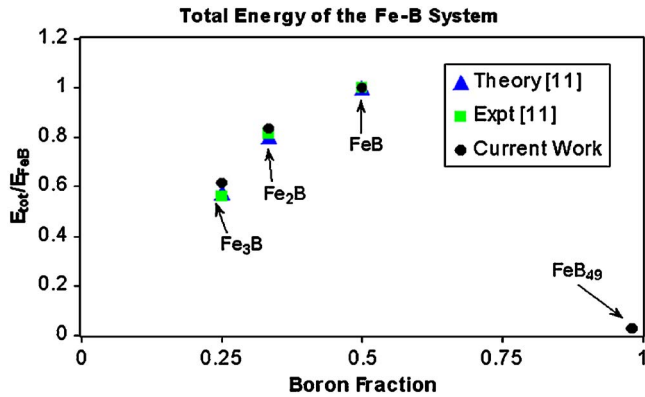


FIG. 3. (Color online) Total-energy calculation via molecular modeling of the Fe-B system using SIESTA 1.3 simulation package.

of FeB phase. This helped to depict the energy variation with change in both iron and boron fractions. Comparison with other work,¹¹ the current study endorses the confidence in predicting the total energy of the newly generated FeB₄₉ phase through modeling software (Table II). Because of the unavailability of the Gibbs free energy, the enthalpy of the Fe₃B phase was approximated to -17.8 kJ/mol (experimental) and -18.3 kJ/mol (theoretical) for the calculation of energy ratio in the comparison studies.

Energy calculations clearly indicate the least stability for FeB₄₉ phase ($E_{tot}/E_{FeB} \sim 0.03$) in Fe-B system. However, the high energy-density laser processing results in the formation of thermodynamically nonequilibrium FeB₄₉ phase corroborating the role of laser processing in producing unconventional phases. Isosurface of (002) plane of FeB₄₉ (Fig. 4) clearly matches with the atomic positions of Fe and B [Fig. 2(b)]. The same plane is stacked twice to depict periodicity and pipe structure observed in the FeB₄₉ crystal.

IV. HIGH-RESOLUTION TRANSMISSION ELECTRON MICROSCOPY

High-resolution TEM imaging captured a thumb structure of growing FeB₄₉ precipitate with smooth matching between two phases, FeB₄₉ and Fe₃B (Fig. 5). Precipitate formed during laser processing, seen in the center as thumb-like structure, has interplanar lattice spacings of 3.68 and 3.05 Å along the two directions, which corresponded to the interplanar spacing of (106) and (302) planes in the FeB₄₉ crystal. The region surrounding FeB₄₉ precipitate has interplanar lattice spacings of 3.53 and 3.06 Å corresponding to the planes (111) and (201) of Fe₃B crystal, respectively. A gradual transition in the mismatch of atomic arrangement

TABLE II. Comparison of total energy of various Fe-B phases.

Phase	E_{tot}/E_{FeB} (Current work)	E_{tot}/E_{FeB} (Ref. 11)	
		Theor.	Expt.
FeB	1.0	1.0	1.0
Fe ₂ B	0.833 98	0.805 03	0.817 61
Fe ₃ B	0.616 77	0.575 47	0.561 01
FeB ₄₉	0.029 89

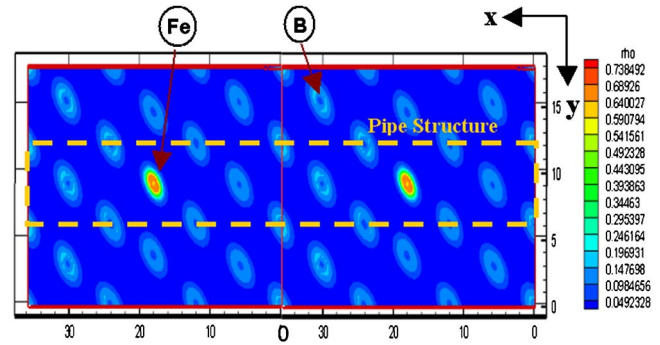


FIG. 4. (Color online) Isosurface density of stacked (002) planes showing crystal continuity and pipe structure in FeB₄₉. Units along the x and y axes are given in bohrs and correspond to rhombohedral geometry. For corresponding pipe structure refer to Fig. 2(b).

along the interface region between Fe₃B and FeB₄₉ phases (Fig. 5) is indicative of mechanically and chemically strong interface between these components. A selected area diffraction (SAD) pattern of the image in Fig. 5 is presented in Fig. 6. The SAD pattern confirmed the presence of Fe₃B and FeB₄₉ phases. The bright diffracted spots corresponded to Fe₃B phase, whereas the weaker (dim) diffraction spots in between the strong diffracted spots corresponded to FeB₄₉.

The formation of metastable phases along the interface depends on the availability of energy for the phase formation. The energy required for a phase formation can be obtained through *ab initio* calculations. Although, *ab initio* calculations are able to predict the final microstructure, the reaction kinetics plays a vital part in the generation of high-energy phases during laser processing. However, molecular simulations for interface characterization and energy calculation remain a prime tool in the prediction of postprocess microstructures.⁷⁻⁹

V. CONCLUSION

Laser surface engineering of TiB₂ coating on 1010 steel generated metastable FeB₄₉ phase, which was characterized through JADE software belonging to $R-3m$ symmetry with lattice parameters of $10.95 \times 10.95 \times 23.86$ Å³. Theoretical x-ray diffraction, constructed via CARINE 3.1 crystallographic

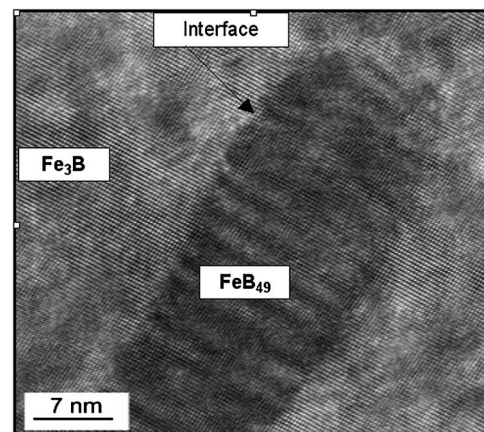


FIG. 5. New phase precipitation as observed through high-resolution TEM imaging.

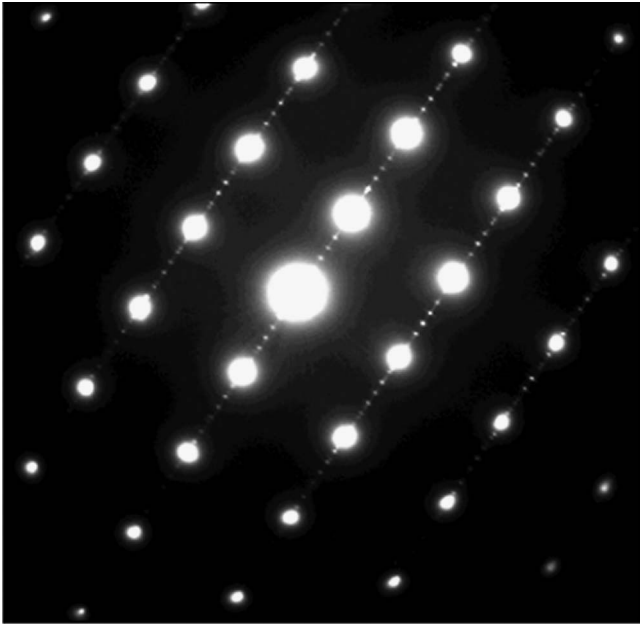


FIG. 6. SAD pattern for Fe_3B and FeB_{49} . Bright diffraction spots represent Fe_3B whereas weak (dim) diffraction spots between bright spots belong to FeB_{49} .

software, was analogous to the experimental peaks, confirming the crystalline nature of the metastable FeB_{49} . *Ab initio* SIESTA 1.3 molecular modeling of Fe–B system corroborated high energy of the FeB_{49} phase. HRTEM depicted smooth interface transition between Fe_3B and FeB_{49} phases dictating the integrity between the two metastable phases. Molecular modeling validated the generation and retention of high-energy phases evolved during the laser surface engineering,

and further, interface modeling of Fe_3B – FeB_{49} remains a challenge for the scientific community to contemplate.

ACKNOWLEDGMENTS

The authors wish to acknowledge Dr. Sukky Jun, Florida International University for providing computing server for running SIESTA 1.3 simulation package. The authors also present their gratitude to A. Garcia, J. Junquera, P. Ordejon, D. Sanchez-Portal, and J. M. Soler for distributing SIESTA 1.3 molecular modeling package and user's guide.

- ¹A. Agarwal and N. B. Dahotre, *Metall. Mater. Trans. A* **31A**, 401 (2000).
- ²A. Agarwal and N. B. Dahotre, *Int. J. Refract. Met. Hard Mater.* **17**, 283 (1999).
- ³B. J. Kooi, Y. T. Pei, and J. Th. M. De Hosson, *Acta Mater.* **51**, 831 (2003).
- ⁴N. B. Dahotre and A. Agarwal, *JOM* **51**, 19 (1999).
- ⁵M. E. Hyman, C. McCullough, J. J. Valencia, C. G. Levi, and R. Meharian, *Mikrochim. Acta* **20A**, 1847 (1989).
- ⁶S. S. Sahay, K. S. Ravichandran, and R. Atri, *J. Mater. Res.* **14**, 4214 (1999).
- ⁷W. Y. Ching, Y. N. Xu, B. N. Harmon, J. Ye, and T. C. Leung, *Phys. Rev. B* **42**, 4460 (1990).
- ⁸M. Palumbo, G. Gacciamani, E. Bosco, and M. Baricco, *Intermetallics* **11**, 1293 (2003).
- ⁹G. Li and D. Wang, *J. Phys.: Condens. Matter* **1**, 1799 (1989).
- ¹⁰A. Agarwal and N. B. Dahotre, *Surf. Coat. Technol.* **106**, 242 (1998).
- ¹¹M. Palumbo, G. Gacciamani, E. Bosco, and M. Baricco, *CALPHAD: Comput. Coupling Phase Diagrams Thermochem.* **25**, 625 (2001).
- ¹²B. D. Cullity, *Elements of X-Ray Diffraction*, 2nd ed. (Addison-Wesley, Philippines, 1978), pp. 504–505.
- ¹³A. G. Jackson, *Handbook of Crystallography for Electron Microscopists and Others* (Springer-Verlag, New York, 1991), pp. 57–74.
- ¹⁴A. Garcia, J. Junquera, P. Ordejon, D. Sanchez-Portal, and J. M. Soler, *SIESTA 1.3 User's Guide*, 1996.
- ¹⁵V. M. Garcia-Suarez, C. M. Newman, C. J. Lambert, J. M. Pruneda, and J. Ferrer, *J. Phys.: Condens. Matter* **16**, 5453 (2004).
- ¹⁶P. Deak, A. Gali, A. Solyom, P. Ordejon, K. Kamaras, and G. Battistig, *J. Phys.: Condens. Matter* **15**, 4967 (2003).